ROYAL SOCIETY
OF CHEMISTRY

PAPER

Check for updates

Enhanced adsorption performance for aromatic sulfur compounds over a hierarchical structured AgX zeolite†

Kunhong Jiang,[a] Zhenyu Li,[ab] Zexuan Zheng,[c] Jiefei Li,[a] Xingyue Qi,[a] Jian Zhou,[a] Hang Wei, [iD][a] Yalin He,[a] Mei Xue [iD] *[a] and Haibin Chu [iD] *[a]

The original NaX zeolite is a promising material for removing organosulfur compounds from fuels. However, its utilization has been challenging owing to its limited adsorption capacity of refractory sulfur compounds. Maintaining the mesoporous structure exposed in hierarchical-NaX is crucial to obtain high desulfurization efficiency. Herein, we synthesize silver supported on hierarchical-X (AgX-CA(3.0)) with abundant mesoporous and adsorption sites to enhance the capacity of adsorption and diffusion of refractory sulfur compounds. The results demonstrate that the adsorbent can be recycled five times without any activity loss, and the framework of the X zeolite is preserved as well. This strategy that introduces mesopores on a hierarchical-NaX to remove organosulfur compounds in the fuel provides a new pathway to limit the emission of sulfur into the atmosphere.

Environmental significance

The combustion of transportation fuels, such as diesel and gasoline, is one of the main sources of SO_x, which is a major air pollutant, which enters the atmosphere and causes acid rain. When gasoline typically exceeds in the order of 1 ppm of sulfur content, it will cause the problem of catalyst poisoning of the fuel cell. Irreversible poisoning of the catalyst in the exhaust gas purification system would increase NO_x emissions. Therefore, the sulfur level must be further reduced to below 1 ppm. In order to protect the environment, almost all countries have issued strict regulations to limit the release of sulfur, which is released into the atmosphere due to the use of fuels.

Introduction

Gasoline fuels are in urgent need of treatment by reducing the organosulfur compound content less than 10 ppm to resolve the serious environmental issue as the combustion of organosulfur compounds can produce SO_2, which will cause pollution by acid rain.[1–3] As a matter of fact, fuel cell catalysts can be toxic when the sulfur content in gasoline generally exceeds 1 ppm.[4,5] Therefore, the sulfur content must be further reduced to below 0.1 ppm.[4] However, the traditional method of hydrodesulfurization (HDS) has shown effectiveness for the removal of high-concentration sulfur such as thiophene (TP), benzothiophene (BT), and their derivatives.[6,7] Its application is limited by operation at harsher conditions of high temperature (300–350 °C) and high hydrogen pressure (2–10 MPa).[8,9] Recently, one particularly effective strategy has been adapted using solid adsorbents to remove organosulfur

compounds and its efficiency is closely related to the choice of the adsorbent. Herein, the new task of developing efficient adsorptive desulfurization (ADS) technology has proposed the need for outstanding adsorption efficiency and stability of adsorbents.[10–12]

At present, various types of porous adsorbents including zeolite,[13–15] activated alumina,[16,17] boron nitride (BN),[18–20] activated carbon (AC),[21,22] and metal–organic frameworks (MOF)[23,24] have been well studied. In particular, the pore diameter of zeolites has been shown to be influential on the ADS efficiency.[12] However, X, Y, and Z zeolites with the advantages of a porous structure and modified surface have been considered to be suitable adsorbents for adsorption desulfurization (ADS).[25–27] However, X and Y zeolites, which have relatively small pore diameter of 1 nm and 0.74 nm, respectively, are unable to remove organic sulfur molecules with a large diameter.[28,29] One option is to achieve hierarchical zeolites, where the microspore-to-mesoporous transition occurs at the zeolite. For example, Al and Si in the zeolite system have been shown to be relatively easily dissolved by acid and alkaline soaking; thus, mesopores inside the zeolites were constructed.[30,31] Yang showed that Ag–Y zeolites are excellent adsorbents for thiophene sulfur removal from benzene owing to the π-complexation interaction between Ag and thiophenic sulfur compounds.[32]

[a]College of Chemistry and Chemical Engineering, Inner Mongolia University, Hohhot, 010021, China. E-mail: setsubai@sina.cn

[b]College of Materials Science and Engineering, Jilin University, Changchun 130022, P. R. China

[c]College of Chemistry, Jilin University, Changchun 130012, PR China

† Electronic supplementary information (ESI) available. See DOI: 10.1039/d1ea00060h

© 2021 The Author(s). Published by the Royal Society of Chemistry

Environ. Sci.: Atmos., 2021, 1, 569–576 | **569**

Herein, we used the template method to construct mesopores inside Ag-hierarchical-X, which can enhance the efficiency of adsorption desulfurization. The mesopores in Ag-hierarchical-X bring about significantly better refractory sulfur compound diffusion relative to the original hierarchical-NaX during the adsorption desulfurization process. As a result, the material can remove 90% of sulfur, which is significantly higher than that of Ag–NaX (60%). Moreover, metal-exchanged zeolite adsorbents are very promising in improving the removal of sulfur compounds.

Experimental section

Materials

Original zeolite NaX (13X) was obtained from Wako Co. Ltd., Japan ($SiO_2/Al_2O_3 = 1.2$). Sulfur compounds, $i.e.$, thiophene (TP), benzothiophene (BT), and 4,6-dibenzothiophene (4,6-DMDBT), were the paraffin constituents of model fuel ($i.e.$, n-heptane). Citric acid (99.9%), ethanol, n-heptane (analytical grade, >99.99%), n-hexadecyltrimethylammonium bromide (98%), nitric acid (70%), silver nitrate (99.8%), and sodium hydroxide (96%) were purchased from Sinopharm Group Chemical Reagent Co., Ltd.

Material characterizations

Powder X-ray diffraction (XRD) patterns of the parent NaX and hierarchically-X were performed on a PANalytical Empyrean diffractometer operating at 40 kV and 40 mA using Cu Kα radiation. The apparent surface area of the zeolites was calculated using the Brunauer–Emmett–Teller (BET) model and the Quantachrome Autosorb instrument. The micropore volume and micropore surface area were calculated by the HK method. The mesopore size of the adsorbents were estimated using the adsorption branch of the isotherm by the BJH model. The H_2 temperature-programmed reduction (H_2-TPR) of the precursors was recorded within the temperature ranging from 100 to 800 °C at a ramp rate of 10 °C min^{-1} by a Micromeritics Auto Chem 2920 analyzer. The intensity and amount of acidic sites existing in the adsorbents were evaluated by the temperature-programmed desorption of ammonia (NH_3-TPD) by a Micromeritics Instrument Corporation-AutoChem II 2920 automatic analyzer. The Scanning Electron Microscopy images of the parent and treated zeolites were obtained using a Hitachi S-4800 at an accelerating voltage of 20 kV. Transmission electron microscopy (TEM) images of the zeolites were acquired on a FEI Tecnai F20 system carried out on an accelerating voltage of 200 kV. The UV-Vis molecular absorption spectrums were recorded by a PerkinElmer UV/Vis/NR Spectrometer Lambda 750. X-ray photoelectron spectroscopy (XPS) analysis was carried out on a THS-103X spectrometer equipped with an Al Kα X-ray source ($hν = 1486.6$ eV).

Preparation of the adsorbent

Preparation of NaX-CA(M). In a typical procedure, original NaX was firstly dealuminated by acid treatment. 3.0 g NaX was dispersed in 30 mL deionized water to form a slurry, in which the pH of the slurry was then adjusted to 5.3–5.5 using 1 M nitric acid solution. 0.5–3.5 mM citric acid (CA) was added into the above slurry and simultaneously stirred for 1 h at ambient temperature. Subsequently, the slurry was filtered and washed thoroughly with deionized water, which then was dried at 333 K for 6 h to get dealuminated NaX. After this, the dealuminated NaX was desiliconized by alkali treatment. 3 g dealuminated NaX was added into 30 mL mixed solution of NaOH (AT, 0.1 M) and CTAB (0.15 M) with vigorous stirring for 24 h at 333 K. After alkali treatment, the slurry was filtered and washed with deionized water, and then dried at 333 K overnight. Furthermore, the sample was calcined at 773 K with a temperature ramp rate of 274.5 K min^{-1} for 2 h in nitrogen atmosphere. After this, the nitrogen was switched to air and then the temperature was increased to 823 K with a temperature ramp of 275 K min^{-1} for 2 h to remove the template (CTAB). The NaX-CA(M) (M is the citric acid concentration) samples were obtained after cooling to room temperature.

Preparation of silver-modified NaX-CA(M). The silver-modified NaX-CA(M) was prepared by the liquid-phase ion-exchange method. NaX-CA(M) (2 g) was added to Ag(I) nitrate solution (0.1 M, 50 mL) under magnetic stirring at ambient temperature for 24 h. Subsequently, the above solution was washed with deionized water and then dried at 333 K. After this, the as-obtained product was calcined at 723 K for 2 h to prepare AgX-CA(M). To avoid the photoreduction of silver species, all the preparation steps were performed in a dark environment.

Adsorption experiment

We also removed physically adsorbed water before the adsorption desulfurization experiment; then, the adsorbents were dried in an oven at 433 K overnight. The adsorption experiments were carried out by batch adsorption method. 10 mL gasoline and 0.1 g adsorbent were mixed in a Teflon tube with stirring at 353 K for 2 h. After the adsorption reaction, the liquid phase supernatant was separated from the adsorbent, and then the sulfur concentration in the supernatant solution was analyzed by UV-visible absorption measurement. The sulfur removal% (S removal%) and adsorption capacity (q_e) were calculated according to the following equation.[33]

$$q_e = \frac{V(C_0 - C_i)}{m} \tag{1}$$

$$\text{S removal } (\%) = \frac{(C_0 - C_i)}{C_0} \times 100\% \tag{2}$$

where V (mL) represents the volume of model gasoline, C_o and C_i (mg per S per L) represent the sulfur concentrations of the model gasoline before and after adsorption, respectively, and m (g) is the mass of the adsorbents.

After adsorption experiments, AgX-CA(3.0) was collected via centrifugation, and then the spent adsorbent was washed with excessive ethanol several times to remove the physically absorbed chemical substances. After this, the obtained sample was calcined at 723 K for 2 h for repeat the test, whose desulfurization performance examination was carried out under the same reaction conditions.

Mathematical model

The pseudo-first order model is given by the equation

$$\mathrm{d}q_t/\mathrm{d}_t = k_1(q_e - q_t) \tag{3}$$

where q_t is the amount of adsorbed sulfur on the adsorbent at time t (min) (mg g^{-1}), q_e is the equilibrium sorption uptake (mg g^{-1}), and k_1 is the pseudo-first order rate constant (min^{-1}). At the boundary conditions, $t = 0$ and $q_t = 0$ to $t = t$ and $q_t = q_t$, the equation takes the form

$$\ln(q_e - q_t) = \ln q_e - k_1 t \tag{4}$$

The pseudo-second order model is

$$\mathrm{d}q_t/\mathrm{d}_t = k_2(q_e - q_t)^2 \tag{5}$$

where q_e is the equilibrium adsorption pseudo-second order adsorption (mg g^{-1}) and k_2 is the pseudo-second order rate constant (g mg^{-1} min^{-1}). The integrated form is:

$$t/q_t = 1/k_2 q_e^2 + t/q_e \tag{6}$$

The Langmuir model explains properties such as physisorption and homogeneous monolayer adsorption. The Langmuir isotherm is represented as

$$\frac{C_e}{q_e} = \frac{1}{q_m K_L} + \frac{C_e}{q_m} \tag{7}$$

where C_e is the remaining concentration of sulfur in the solution at equilibrium (mg L^{-1}) and q_m is the theoretical maximum adsorption capacity (mg g^{-1}), representing the monolayer coverage amount of the adsorbents.[34] K_L reflects the strength of adsorption and q_e is the amount of sulfur adsorbed at equilibrium (mg g^{-1}).

Results and discussion

The preparation of hierarchical-AgX (AgX-CA(3.0)) with a meso–microporous structure includes the synthesis of NaX-CA(3.0) and the process of their subsequent ion exchange. Firstly, NaX-CA(3.0) was synthesized by sequential acid–alkali treatment method, in which Al and Si were removed from the original faujasite zeolite NaX. After this, followed by the ion exchange method between AgX-CA and Ag ion, the AgX-CA(3.0) zeolite adsorbent was obtained (Scheme 1). For comparison, we also synthesized the AgX adsorbent by a similar experiment process except for the step of sequential acid–alkali treatment. As shown in Fig. 1a, the XRD pattern of the original NaX, NaX-CA(3.0), AgX, and AgX-CA(3.0) adsorbents shows the characteristic peaks of X zeolite with a faujasite (FAU) topology, indicating that all the adsorbents maintain the structure of the conventional zeolite. Compared with NaX-CA(3.0) and NaX, the (111) peak intensity of AgX-CA(3.0) and AgX decrease with the addition of citric acid during the acid–alkali treatment process, respectively. This result may be attributed to the partial collapse of the NaX framework and the breakage of the Al–O and Si–O bonds.[35,36] Besides, the XRD pattern of AgX-CA(3.0) is similar to
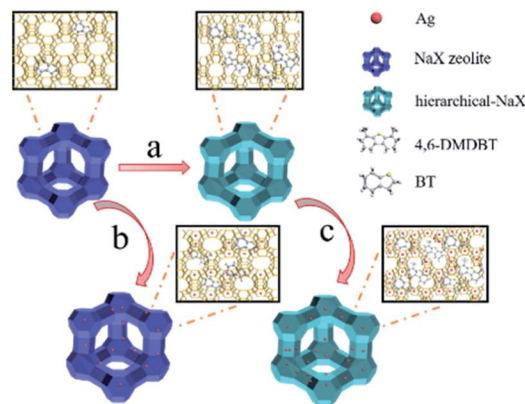
Scheme 1 Schematic illustration of the design for the synthesis of hierarchical-AgX. (a) Sequential acid–alkali treatments of NaX; (b) silver supported on original NaX; (c) silver supported on hierarchical NaX after sequential acid–alkali treatments.

that of NaX-CA(3.0), indicating that the NaX structure is retained and no diffraction peaks related to Ag$_2$O (JCPDS no. 65-3289) is observed. This result demonstrated that the silver species are possibly well dispersed on the X zeolite. Further, it was interesting to note that the diffraction peak disappeared at 10° and a new peak appeared at 14° for AgX-CA(3.0), revealing that the incorporation of silver may induce electronic densities of NaX and redistribute the charge of NaX.[36]

To attain the valence of Ag species in the AgX-CA(3.0) sample, X-ray photoelectron spectroscopy (XPS) measurement was carried out with the AgX-CA(3.0) zeolite adsorbent. As
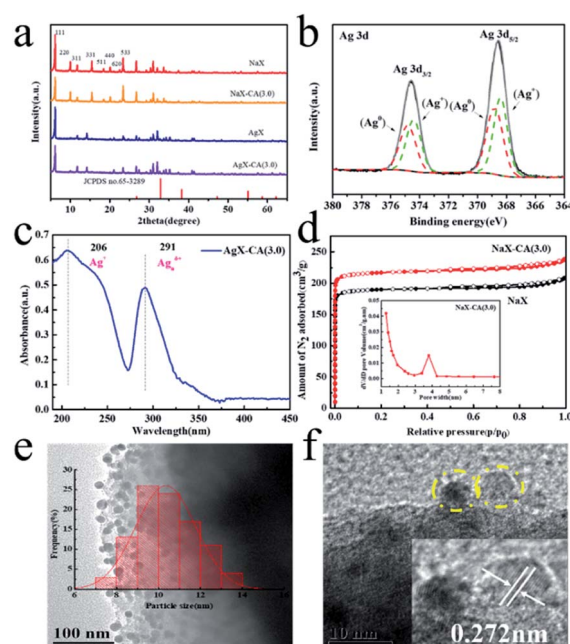

Fig. 1 (a) XRD patterns of NaX, NaX-CA(3.0), AgX, and AgX-CA (3.0), (b) XPS spectra, (c) UV-vis spectrum of AgX-CA. (d) N$_2$ adsorption isotherms of NaX-CA(3.0) and NaX. (e) TEM and (f) HRTEM images of AgX-CA.

© 2021 The Author(s). Published by the Royal Society of Chemistry

Environ. Sci.: Atmos., 2021, **1**, 569–576 | **571**

illustrated in Fig. 1b, the Ag 3d XPS spectra of the AgX-CA(3.0) zeolite adsorbent exhibits two main peaks centered at 368.2 and 368.8 eV, which are consistent with Ag $3d_{5/2}$ and Ag $3d_{3/2}$, respectively. This result demonstrates that the AgX-CA(3.0) zeolite adsorbent has two valence states corresponding to metallic Ag^0 and ionic Ag^+.[37–41] As displayed in Fig. 1c, the UV-visible absorption spectrum of AgX-CA(3.0) exhibits characteristic absorption bands at about 206 nm and 291 nm, which may be attributed to the electronic transition of highly dispersed Ag(ɪ) ions and a small cluster of $Ag_n^{\delta+}$, respectively.[37,40–42] There is no absorption of nano Ag_2O in the visible light area. Based on the above results, we can infer that the Ag species of AgX-CA(3.0) has two types of loading, one is the isolated Ag cations on the surface of the X zeolite particles, and the other is the Ag cations, which are embedded in the pores of the X zeolite.

The existence of a microporous structure in the NaX-CA(3.0) adsorbent is explained by the N_2 adsorption–desorption isotherms and pore size distribution plot in Fig. 1d. Both the samples display IUPAC type I, suggesting that it is a typical microporous material.[43] Compared with NaX, NaX-CA(3.0) shows enhanced N_2 uptake at a lower relative pressure, indicating that the total pore volume is increased. The pore size distribution of NaX-CA(3.0) displays a newly created microporous structure with a pore diameter of 3.8 nm. Under the presence of the CTAB surfactant, the partial framework of NaX-CA is orderly destroyed by sequential acid–alkali treatments, resulting in a structure of micropores and secondary mesopores whose pore diameter matches with that of the CTAB micelles.[35] The pore structure parameters of the samples are shown in Table S1.† Compared with the original NaX, NaX-CA(3.0) exhibits a higher mesopore surface area (43.06 m^2 g^{-1}) and mesopore volume (34.01 m^3 g^{-1}). The mesopores introduced into NaX-CA(3.0) may be due to sequential acid–alkali treatments, resulting in Al and Si element extraction from NaX, and the partial micropore structure of NaX is destroyed and then the mesopores are formed. The mesopores of 3.9 nm will accelerate the diffusion of organic sulfide molecules (TP: 0.56 × 0.77 nm BT: 0.65 × 0.89 nm and 4,6-DMDBT: 0.78 × 1.23 nm),[44] while allowing them to easily enter into the zeolite pores and interact with the metal ion active sites, thus improving the desulfurization performance.

The SEM images of the original NaX and NaX-CA(3.0) are shown in Fig. S1.† The NaX sample shows a cubic particle shape and irregular polyhedral crystal structure, and the particle width is approximately 2–5 μm. Unlike NaX, the surface of NaX-CA(3.0) becomes rough, which may be due to the extraction of Al and Si elements from NaX by sequential acid–alkali treatments. Furthermore, in order to get insights into the unique structure of AgX-CA(3.0), the TEM image of AgX-CA(3.0) has been shown (Fig. 1e). The numerous nanoparticles with an almost uniform size distribution are observed over the AgX-CA sample. The average particle size, as observed for AgX-CA, is 1.67 nm within the range of 6–10 nm after Ag modification. The high-resolution TEM (HRTEM) image of AgX-CA shows the presence of a lattice fringe spacing of 2.72 Å, which is in good agreement with the Ag_2O (111) facets (Fig. 1f). The Ag_2O phase is not detected in the XRD analysis (Fig. 1a), indicating that the Ag_2O nanoparticles

are well dispersed on AgX-CA(M), which is in good agreement with the results of TEM analysis.

The Si, Al, and Ag content of the adsorbents were estimated by EDS measurement (Fig. S2†). The Si/Al molar ratio of AgX-CA(3.0) is 1.17, which is higher than that of AgX (1.03). This result suggests that Al and Si can be removed by the acid–alkali treatments process, which would inevitably leave many vacancies and enlarge the surface area of the NaX-CA(3.0) sample.[45] The Ag atomic percentages of AgX and AgX-CA(3.0) are 5.35 and 8.76, respectively, suggesting the successful loading of Ag in the AgX-CA(3.0) sample.

A deeper insight of Ag species distribution was obtained through the desorption peaks from the temperature-programmed reduction (TPR) of all the samples. As shown in Fig. 2a, there are four typical desorption peaks that can be observed. Note that the characteristic peaks at 120 °C are also observed due to the partial reduction of Ag_2O on the zeolite surface by H_2. The peaks at about 220 °C correspond to Ag_2O clusters located in the supercage of the X zeolite,[46,47] and a lower temperature means more ease of adsorption desulfurization.[48,49] Interestingly, the peaks at 120 °C and 220 °C of AgX-CA(M) obviously shift to a low temperature with the increase in the concentration of citric acid, suggesting easier hydrogen release from AgX-CA(M) due to the presence of mesopores on its surface.[49,50] This means that the presence of a mesoporous structure on the zeolite surface can effectively allow the organic sulfur compounds of thiophene to diffuse and interact with the Ag_2O nanoparticles inside the zeolite. Furthermore, the peak at about 300 °C is assigned to small Ag clusters inside the sodalite cages of zeolite.[50,51] The peak quantity of AgX, AgX-CA(1.5), AgX-CA(2.0), and AgX-CA(3.0) is 13.07, 12.52, 13.21, and 17.40 mmol g^{-1}, respectively (Table S2†). This result indicates the role of the mesoporous structure on the AgX-CA(3.0) surface as possessing a higher Ag loading amount than those of AgX, which is consistent with the EDS results (Fig. S2†). In particular, the hydrogen consumption peak at 410 °C is only observed for the AgX-CA(3.0) sample, suggesting the existence of Ag ion.[51,52] Based on the H_2-TPR and UV-vis results, we can infer that silver oxide clusters and Ag ion are mainly dispersed on the external surface and the internal pores of the X zeolite, respectively. Besides, the hierarchical structure of NaX-CA (3.0) can effectively enhance the Ag ion loading and facilitate Ag ion distribution in the X zeolite.[53,54]
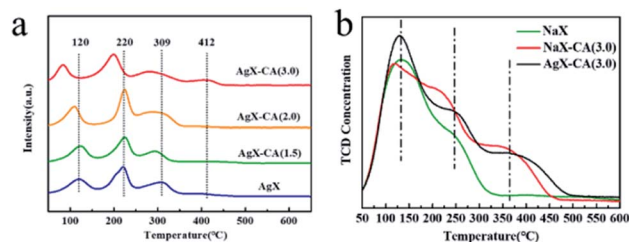

Fig. 2 (a) H_2-TPR spectra of AgX and AgX-CA(M). (b) NH_3-TPD patterns of NaX, NaX-CA(3.0), and AgX-CA(3.0) adsorbents.

To gain the zeolites acidity fingerprint, the NH$_3$-TPD analysis of original NaX, NaX-CA(3.0), and AgX-CA(3.0) were collected. The acidic sites are generally classified into three types including weak acidity (136 °C), moderate acidity (200–300 °C), and strong acidity (>300 °C).[55–57] As shown in Fig. 2b, three clear peaks can also be observed. These peaks arise at 130 °C and 260 °C for original NaX, indicating that weak acidic sites and moderately strong acid sites are present in the NaX zeolite.[58] NaX-CA(3.0) exhibits a new desorption peak at about 360 °C after acid treatment for the NaX zeolite. When the Ag ion is subsequently exchanged, the intensity at about 360 °C is obviously increased, which stated that the acid–alkali treatments and the addition of Ag could enhance the acidity of the NaX zeolite. Therefore, the amount of strong acidic sites of the samples increases in the following order NaX (2.50 mmol g^{-1}) < NaX-CA(3.0) (3.66 mmol g^{-1}) < AgX-CA(3.0) (3.83 mmol g^{-1}). Also, based on the previous report that higher Ag are exchanged, larger NH$_3$ concentration is retained.[59] By comparison of the peak areas of the spectra of the respective zeolites, the acid site number of the NaX-CA(3.0) sample is increased due to newly created mesopores on its surface.[37] As for the AgX-CA(3.0) sample, this increase in the amount of desorbed NH$_3$ is probably related to the creation of new acid sites because of the highly dispersed Ag$_2$O clusters in the pores of the X zeolites. Also, in the following results, the acidic property of adsorbents caused some differences in their adsorption desulfurization performance.

Adsorptive desulfurization performance

Desulfurization of model gasoline. The adsorptive desulfurization performances of AgX, AgX-CA(1.5), AgX-CA(2.0), and AgX-CA(3.0) were also performed using *n*-heptane as the solvent, thiophene and methylbenzene as the substrate to

Fig. 3 (a) Adsorptive desulfurization performance of AgX and AgX-CA(M) from model gasoline. (b) Kinetic plots at different temperatures for adsorption BT onto AgX-CA(3.0). (c) Sorption isotherms for BT by AgX-CA(3.0) adsorbent. (d) Sorption isotherms for 4,6-DMDBT by AgX-CA(3.0) adsorbent. Experimental conditions: Initial sulfur concentration was 20 ppm, vol. (model gasoline) = 10 mL, wt (adsorbent) = 0.1 g, temperature: 80 °C, contact time: 2 h.

model the gasoline with low sulfur concentration. It is worth noting that the sulfur removed from gasoline for most of the adsorbents typically suffers at higher temperature (80 °C) because gasoline contains lower sulfur concentration. As shown in Fig. 3a, the desulfurization capacity of AgX-CA(3.0) is 85.48%, which is higher than those of AgX (59.67%), AgX-CA(1.5) (75.15%), and AgX-CA(2.0) (80.87%). Moreover, the removed capacity of DMDBT for AgX-CA(3.0) is 99.09%, which is higher than those of AgX (61.15%), AgX-CA(1.5) (89.64%), and AgX-CA(2.0) (97.87%). For both the sulfides, the AgX-CA(3.0) exhibited rather higher desulfurization capacity than those of AgX, AgX-CA(1.5), and AgX-CA(2.0). The much higher desulfurization capacity of AgX-CA(3.0) can be attributed to the increased Ag$^+$ and citric acid concentration.

Besides, the desulfurization performance of NaX-CA(M) is also shown in Fig. S3;† the NaX-CA(3.0) sample with a higher specific surface area and more mesopores shows the largest sulfur capacity, suggesting that the mesopores are favorable for BT and 4,6-DMDBT molecule diffusion and then the sulfur removal is enhanced. One of the reasons for this enhancement is physical adsorption. According to previous reports, the overlapping of the potential field from the micropore walls will increase the adsorption of electron-rich adsorbates, which is called the "micropore filling effect".[60,61] Nevertheless, this physical adsorption is not selective for thiophene. Another possible reason for sulfur removal enhancement is the difference in the organic sulfur compound's molecular steric hindrance.[57] As is known, the supercage size of the original NaX zeolite is 0.9 nm, which is slightly larger than the critical diameter of TP (0.56 × 0.77), equalling that of BT (0.65 × 0.89) and smaller than 4,6-DMDBT (0.78 × 1.23). Therefore, the diffusion of BT or 4,6-DMDBT molecule into the NaX pores is relatively difficult.[62] NaX-CA(3.0) shows newly created mesopores with a diameter of 3.9 nm, promoting BT and 4,6-DMDBT molecule distribution, thus, these aromatic sulfur compounds can enter into the pores.

For AgX-CA(3.0), due to the π-complexation interaction between Ag$^+$ and aromatic sulfur compounds, the Ag$^+$ active site can increase the selectivity and activity of the TP derivatives. Yang *et al.*[63] determined that Ag-exchanged Y zeolites can adsorb thiophene through π-complexation between the sulfur compounds and Ag, and thus exhibit high capacities of desulfurization. The sulfur removal capacity of the adsorbents is influenced by the metal ion loading. Higher Ag ion-exchange level and mesopores are beneficial for desulfurization performance.

In order to gain a better understanding of the adsorption process of BT onto the Ag-loaded modified adsorbent (AgX-CA(3.0)), the kinetic models were used to test the experimental data.[64] For this purpose, pseudo-first-order and pseudo-second-order models were used to describe and analyze the kinetics of the adsorption process over the AgX-CA(3.0) sample. In the following, the two adsorption kinetic models were evaluated to fit the kinetics of the adsorption process onto AgX-CA(3.0) with BT. The non-linear fitting curves of the three temperature (30, 50, and 80 °C) adsorption kinetic models are shown in Fig. 3b, and related parameters are shown in Table S3.† The pseudo-second-order model seems to be better than the pseudo-first-order model. When BT is adsorbed by the AgX-
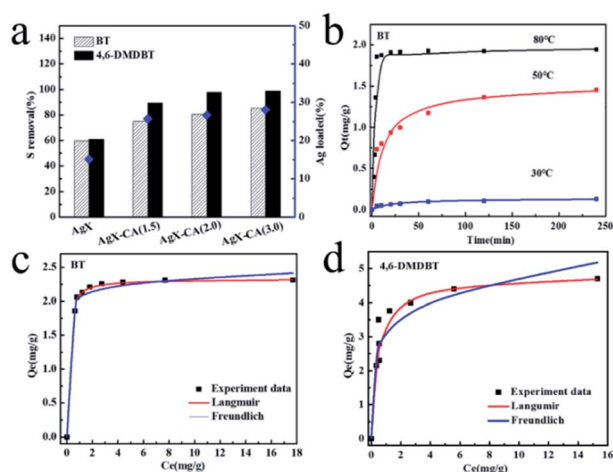
© 2021 The Author(s). Published by the Royal Society of Chemistry

Environ. Sci.: Atmos., 2021, **1**, 569–576 | **573**

CA(3.0) zeolite, the pseudo-second-order model regression coefficient at different temperatures is about 0.99, demonstrating that the experimental data meets the pseudo-second-order model very well, and when adsorbed at 80 °C, the pseudo-second-order rate constant k_2 is 0.204 min^{-1} and the equilibrium adsorption amount (q_e) reaches 1.967 mg g; it can be obviously found that the q_e and k_1 of BT for the AgX-CA(3.0) zeolite increased with increasing temperature; when the contact time is the same, the higher the temperature is, the greater the q_t becomes, showing that the higher temperature is beneficial for the adsorption process. The higher temperature usually has a major impact on the adsorption process by the increase in the diffusion rate of the adsorbate greatly and leads to a greater equilibrium capacity. The adsorption rate of sulfur compounds on AgX-CA(3.0) becomes faster with temperature increase, indicating that the activation energy of the substances can be decreased on the adsorbent surface.[65]

The equilibrium behavior was described by equilibrium isotherms investigated based on batch experiments. Each isotherm curve was analyzed using Langmuir and Freundlich adsorption models. In all the cases, the isotherms are better fitted to the Langmuir isotherm model. The equilibrium parameters are given in Table S4.† The relation $n > 1$ indicates favorable adsorption. It can be seen that the q_m of the prepared adsorbent reached 2.32 mg g^{-1} (BT) and 4.81 mg g^{-1} (4,6-DMDBT).

Regeneration performance of the AgX-CA(3.0) adsorbents

To assess the recyclability of the catalysts of the AgX-CA(3.0) adsorbent, the degradation tests were performed 5 times. As shown in Fig. 4a, the AgX-CA(3.0) adsorbent, without a loss of the activity after 5 times recycling, exhibits much higher stability. Unlike AgX-CA(3.0), the activities of AgX, AgX-CA(1.5), AgX-CA(2.0), and AgX-CA(3.0) show significant degradation *via* the metal agglomeration effect, which highlights the obstacle of the sustainability catalysts for desulfurization at a large scale. As displayed in Fig. 4b, the XRD patterns of the used AgX-CA(3.0) adsorbent do not have obvious changes, suggesting that the crystal structure can be well retained and is not influenced by cyclic desulfurization.

Discussion

On the basis of the experiment above, the as-synthesized AgX-CA(3.0) (99.09%) exhibits higher adsorption desulfurization performance and durability than those of AgX (61.15%), AgX-CA(1.5) (89.64%), and AgX-CA(2.0) (97.87%). The superb adsorption desulfurization performance of AgX-CA(3.0) mainly arises from the following aspects: (i) the hierarchical pore structure effect. Compared with NaX, NaX-CA(3.0) showed a newly created microporous structure with a pore diameter of 3.8 nm. Moreover, compared with original NaX, NaX-CA(3.0) exhibited higher mesopore surface area (43.06 m^2 g^{-1}) and mesopore volume (34.01 m^3 g^{-1}). The desorption peaks from the TPR of AgX-CA(3.0) shifted to a low temperature and the amount of desorbed NH$_3$ increased from TPD, which suggested that the hierarchical structure of AgX-CA(3.0) can effectively enhance the Ag ion loading and facilitate Ag ion distribution in the X zeolite. (ii) The interaction effect. The Ag$^+$ active site can increase the selectivity and activity of the TP derivatives due to π-complexation interaction between Ag$^+$ and aromatic sulfur compounds. The experimental results are consistent and confirm that the hierarchical pore structure and the increased Ag$^+$ active site are effective in improving the adsorption desulfurization performance of NaX materials. In addition, the desulfurization capacity of AgX-CA(3.0) shows nearly no loss after 5 times cycling, which can be attributed to the retained crystal structure.

Atmospheric implications

The combustion of transportation fuels such as diesel and gasoline releases huge amounts of sulfur oxides (SO$_x$) into the atmosphere. Excess sulfur dioxide in the atmosphere leads to air pollution and even acid rain. Besides, the presence of sulfur compounds in fuels corrodes petroleum refinery equipment and poisons catalytic converters, which are the main devices that control automotive emission. Zeolites can effectively adsorb and remove H$_2$S toxic substances, and then they have excellent regenerability and stable structure during the catalytic process.[66] In order to protect the atmosphere and realize zeolites' more excellent adsorption property, we have synthesized the mesoporous AgX-CA(3.0) adsorbent by dealumination and desilication, followed by the metal-exchange method. The mesoporous AgX-CA(3.0) adsorbent not only inherits the original active sites of Ag but also retains the frame and microporosity of the zeolites. The as-prepared mesoporous AgX-CA(3.0) exhibits outstanding sulfur adsorptive performance. The experimental results showed that the removal capacity of 4,6-DMDBT for AgX-CA(3.0) was 99.09% and BT is 85.48%, which is 1.4 and 1.6 times higher than those of AgX (61.15% and 59.67%), respectively. This synthetic strategy gives a new opportunity for the preparation of efficient desulfurization adsorbent, and then contributes to the protection of the atmosphere.

Conclusions

We have successfully prepared hierarchical-X zeolite adsorbent NaX-CA(M) by sequential acid–alkali treatment with tunable acidity. The experimental results show that the surface area and pore volume of the NaX-CA(M) mesopore were fully increased,
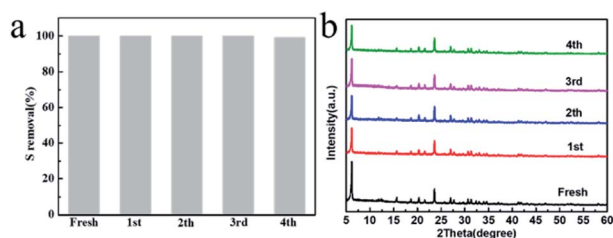

Fig. 4 (a and b) Powder XRD patterns for the as-prepared and used (after 1, 2, 3, and 4 cycles) AgX-CA(3.0) adsorbent.

leading to enhanced desulfurization performance for thiophene sulfur compounds with a large molecular size. Moreover, silver is further supported on the AgX-CA(M) to improve the sulfur capacity. This enhancement is driven by the silver metal, which can create active sites to bind with aromatic sulfur compounds *via* π-complexation. The sequential acid–alkali treatment promotes silver metal to diffuse and load into hierarchical-X zeolites, increasing the amount of acidic sites. The preparation of the hierarchical X zeolite adsorbent provides a meaningful strategy to obtain high performance for the removal of molecules large sulfur compounds.

Conflicts of interest

There are no conflicts to declare.

Acknowledgements

Notes and references

1 C. Lamonier, *Nat. Energy*, 2017, **2**, 17019.
2 A. Toutov, M. Salata and A. Fedorov, *Nat. Energy*, 2017, **2**, 17008.
3 L. D. Hao, S. A. Stoian and L. R. Weddle, *Green Chem.*, 2020, **22**, 6351–6356.
4 M. Xue, R. Chitrakar and F. Qi, *J. Colloid Interface Sci.*, 2005, **2**, 487–492.
5 Y. Zu, Z. S. Guo and L. J. Song, *Chem. Eng. J.*, 2020, **308**, 122319.
6 L. Hao, J. J. Liu and J. C. Li, *ACS Catal.*, 2017, **7**, 4805–4816.
7 P. S. Kulkarni and C. A. M. Afonso, *Green Chem.*, 2010, **12**, 1139–1149.
8 D. Yang and B. C. Gates, *ACS Catal.*, 2019, **9**, 1779.
9 S. Zhao, H. Yi and X. Tang, *J. Hazard. Mater.*, 2018, **344**, 797–810.
10 N. A. Khan and S. H. Jhung, *Angew. Chem., Int. Ed.*, 2012, **51**, 1198–1201.
11 T. Wang, X. Li and W. Dai, *J. Mater. Chem. A*, 2015, **3**, 21044–21050.
12 K. X. Lee and J. A. Valla, *Appl. Catal., B*, 2017, **201**, 359–369.
13 C. Yang, X. Meng and D. Z. Yi, *Ind. Eng. Chem. Res.*, 2019, **58**, 1613–1623.
14 A. J. Hernandez-Maldonado and R. T. Yang, *Ind. Eng. Chem. Res.*, 2003, **42**, 123–129.
15 Y. X. Li, J. X. Shen, S. S. Peng and L. B. Sun, *Nat. Commun.*, 2020, **11**, 3206.
16 L. B. Qin, Y. S. Zhou and D. Q. Li, *Ind. Eng. Chem. Res.*, 2016, **55**, 7249–7258.
17 A. Srivastav and V. C. Srivastava, *J. Hazard. Mater.*, 2009, **170**, 1133–1140.
18 J. Xiong, L. Yang and Y. Chao, *ACS Sustainable Chem. Eng.*, 2016, **4**, 4457–4464.
19 P. W. Wu and W. Shuai, *Chem. Commun.*, 2016, **52**, 144–147.
20 J. Xiong, W. Zhu and H. Li, *Green Chem.*, 2015, **17**, 1647–1656.
21 Y. Wang and R. T. Yang, *Langmuir*, 2007, **23**, 3825–3831.
22 T. A. Saleh, K. O. Sulaiman, S. A. Al-Hammadi, H. Dafalla and G. I Danmaliki, *J. Cleaner Prod.*, 2017, **154**, 401–412.
23 J. X. Qin, P. Tan, Y. Jiang, X. Q. Liu, Q. X. He and L. B. Sun, *Green Chem.*, 2016, **18**, 3210.
24 L. M. Rodríguez-Albelo, E. López-Maya and S. Hamad, *Nat. Commun.*, 2017, **8**, 14457.
25 E. Díaz, S. Ordóñez, A. Vega and J. Coca, *Microporous Mesoporous Mater.*, 2005, **83**, 292–300.
26 A. Inayat, C. Schneider and W. Schwieger, *Chem. Commun.*, 2015, **51**, 279–281.
27 J. García-Martínez, M. Johnson, J. Valla, K. Li and J. Y. Ying, *Catal. Sci. Technol.*, 2012, **2**, 987–994.
28 M. Hartmann, A. G. Machoke and W. Schwieger, *Chem. Soc. Rev.*, 2016, **45**, 3313–3330.
29 S. Lopez-Orozco, A. Inayat, A. Schwab, T. Selvam and W. Schwieger, *Adv. Mater.*, 2011, **23**, 2602–2615.
30 H. Z. Li, L. X. Dong, L. Zhao, L. Y. Cao, J. S. Gao and C. M. Xu, *Ind. Eng. Chem. Res.*, 2017, **56**, 3813–3821.
31 Y. L. Jiao, L. Forster and S. J. Xu, *Angew. Chem., Int. Ed.*, 2020, **59**, 19478–19486.
32 A. J. Hernandez-Maldonado and R. T. Yang, *Ind. Eng. Chem. Res.*, 2004, **43**, 769–776.
33 Q. Y. Zhu, G. D. Moggridge and M. Ainte, *Chem. Eng. J.*, 2016, **306**, 67–76.
34 H. Song, B. L. Jiang, H. L. Song, Z. S. Jin and X. L. Sun, *Res. Chem. Intermed.*, 2015, **41**, 3837–3854.
35 X. Y. Ren, J. P. Cao, X. Y. Zhao, Z. Yang, S. N. Liu and X. Y. Wei, *ACS Sustainable Chem. Eng.*, 2018, **6**, 1792–1802.
36 W. Li, J. Zheng, Y. Luo, C. Y. Tu, Y. Zhang and Z. J. Da, *Energy Fuels*, 2017, **31**, 3804–3811.
37 M. Chebbi, B. Azambre, L. Cantrel and T. Albiol, *Microporous Mesoporous Mater.*, 2017, **224**, 137–150.
38 G. B. Hoflund and Z. F. Hazos, *Phys. Rev. B: Condens. Matter Mater. Phys.*, 2000, **62**, 11126–11133.
39 G. K. Wertheim, J. H. Wernick and S. Hufner, *Solid State Commun.*, 1975, **17**, 417–422.
40 A. Jezierski, A. Szytula, B. Penc and D. Fus, *J. Alloys Compd.*, 2001, **317**, 340–346.
41 L. Ferreira, A. M. Fonseca, G. Botelho, C. A. Aguiar and I. C. Neves, *Microporous Mesoporous Mater.*, 2012, **160**, 126–132.
42 M. Chebbi, B. Azambre and L. Cantrel, *J. Phys. Chem. C*, 2016, **120**, 222–295.
43 A. Al-Ani, R. J. Darton and S. Sneddon, *ACS Appl. Nano Mater.*, 2018, **1**, 310–318.
44 J. Pérez-Ramírez, C. H. Christensen, K. Egeblad, C. H. Christensen and J. C. Groen, *Chem. Soc. Rev.*, 2008, **37**, 2530–2542.
45 Z. Qin, K. A. Cychosz, G. Melinte, H. E. Siblani, J. P. Gilson, M. Thommes, C. Fernandez, S. Mintova, O. Ersen and V. Valtchev, *J. Am. Chem. Soc.*, 2017, **139**, 17273–17276.
46 H. Song, X. Wan and M. Dai, *Fuel Process. Technol.*, 2013, **116**, 52–62.

© 2021 The Author(s). Published by the Royal Society of Chemistry

Environ. Sci.: Atmos., 2021, **1**, 569–576 | **575**

47 W. Henao-Sierra, M. Romero-Sáez and F. Gracia, *Microporous Mesoporous Mater.*, 2018, **265**, 250–257.

48 H. Y. Zheng, J. Z. Wang and Z. Li, *Fuel Process. Technol.*, 2016, **152**, 367–374.

49 Q. Tang, Y. Wang and Q. Zhang, *Catal. Commun.*, 2003, **4**, 253–258.

50 S. W. Baek, J. R. Kim and S. K. Ihm, *Catal. Today*, 2004, **93**, 575–581.

51 E. Kolobova, A. Pestryakov and G. Mamontov, *Fuel*, 2017, **188**, 121–131.

52 M. F. Ribeiro, R. Bartolomeu and A. N. Mendes, *Catal. Sci. Technol.*, 2016, **6**, 3038–3048.

53 G. R. Eulenberger, D. P. Shoemaker and J. G. Keil, *J. Phys. Chem. C*, 1967, **71**, 1812–1819.

54 N. D. Hutson, B. A. Reisner and R. T. Yang, *Chem. Mater.*, 2000, **12**, 1067–1073.

55 S. A. Skarlis, D. Berthout and N. André, *J. Phys. Chem. C*, 2012, **116**, 8437–8448.

56 Q. Y. Cai, G. X. Hou and D. L. Hai, *Acta Phys.-Chim. Sin.*, 2014, **30**, 544–550.

57 H. Song, Y. X. Chang and H. L. Song, *Adsorption*, 2016, **22**, 139–150.

58 C. S. Triantafillidis, A. G. Vlessidis and N. P. Evmiridis, *Ind. Eng. Chem. Res.*, 2000, **39**, 307–319.

59 F. Benaliouche, Y. Boucheffa and P. Ayrault, *Microporous Mesoporous Mater.*, 2007, **111**, 80–88.

60 J. Garcia-Martinez, K. Li and G. Krishnaiah, *Chem. Commun.*, 2012, **48**, 11841–11843.

61 D. Fodor, F. Krumeich, R. Hauert and J. van Bokhoven, *Chem.–Eur. J.*, 2015, **21**, 6272–6277.

62 Y. X. Li, W. J. Jiang and P. Tan, *J. Phys. Chem. C*, 2015, **119**, 21969–21977.

63 R. T. Yang, A. J. Hernández-Maldonado and F. H. Yang, *Science*, 2003, **301**, 79–81.

64 J. F. Li, H. Gyoten, A. Sonoda, Q. Feng and M. Xue, *RSC Adv.*, 2017, **7**, 1490–1497.

65 I. Muhammad, S. Siraj, A. Imtiaz, U. Hameed, Y. Muhammad and A. Alia, *J. Saudi Chem. Soc.*, 2017, **21**, 143–151.

66 M. Ozekmekci, G. Salkic and M. F. Fellah, *Fuel Process. Technol.*, 2015, **139**, 49–60.